eLIFE elifesciences.org

RESEARCH ARTICLE

Figures and figure supplements

Therapeutic effects of telomerase in mice with pulmonary fibrosis induced by damage to the lungs and short telomeres

Juan Manuel Povedano *et al*

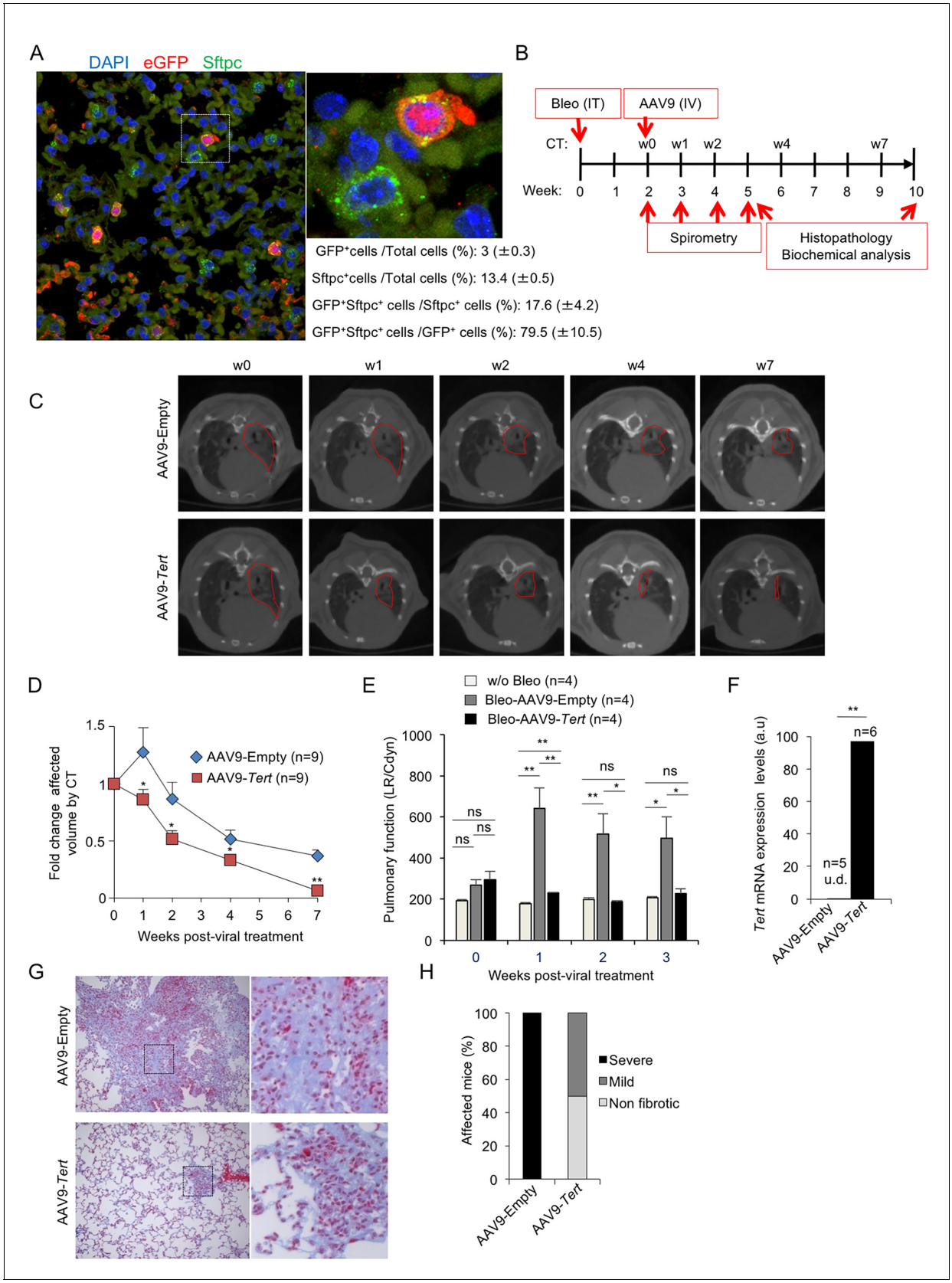

Figure 1. AAV9-*Tert* treatment targets ATII cells leading to remission of pulmonary fibrosis. (**A**) Representative image of immunofluorescence against eGFP (in red) and Sftpc (in green). Mice were injected intravenously in the tail with AAV9-*eGFP* and sacrificed two weeks later to determine virus cell

Figure 1 continued on next page

Figure 1 continued

type target. The quantification of percentage of GFP^+ $Sftpc^+$ cells relative to total GFP^+ cells and to total $Sftpc^+$ cells is shown. (**B**) Eight-ten week old male G2*Tert*$^{-/-}$ mice were intratracheally inoculated with 0.5 mg/kg BW bleomycin and two weeks after computed tomography (CT)-diagnosed with pulmonary fibrosis (PF). Affected mice were treated intravenously either with AAV9-empty or AAV9-*Tert*. Spirometric follow–up was performed at 1, 2 and 3 weeks post-viral treatment with the viral vectors. CT follow-up was performed at 1, 2, 4 and 7 weeks post-treatment with the viral vectors. Mice were sacrificed at 3 and 8 weeks post-treatment with the viral vectors for further biochemical and histopathological lung examination. (**C**) CT representative images for every time point of the treatment (fibrotic area in red). (**D**) Quantification of fold change affected lung volume with PF normalized to the affected volume before the viral treatment by computed tomography (CT). (**E**) Follow-up of pulmonary function measured as the ratio between lung resistance and dynamic compliance (LR/Cdyn) (**F**) *Tert* transcriptional levels in lung 8 weeks post-viral treatment. a.u., arbitrary units (**G**) Masson´s trichrome staining from lung sections to evaluate fibrotic regions at end point 8 weeks post-viral treatment (collagen fibers in blue; nuclei and erythrocytes in red). (**H**) Histopathological analysis and fibrosis score from lung sections at end point. The number of mice analyzed per group is indicated. T-test was used in D, E and F and χ^2 analysis in H and I for statistical analysis. *p=0.05; **p<0.01.

DOI: https://doi.org/10.7554/eLife.31299.003

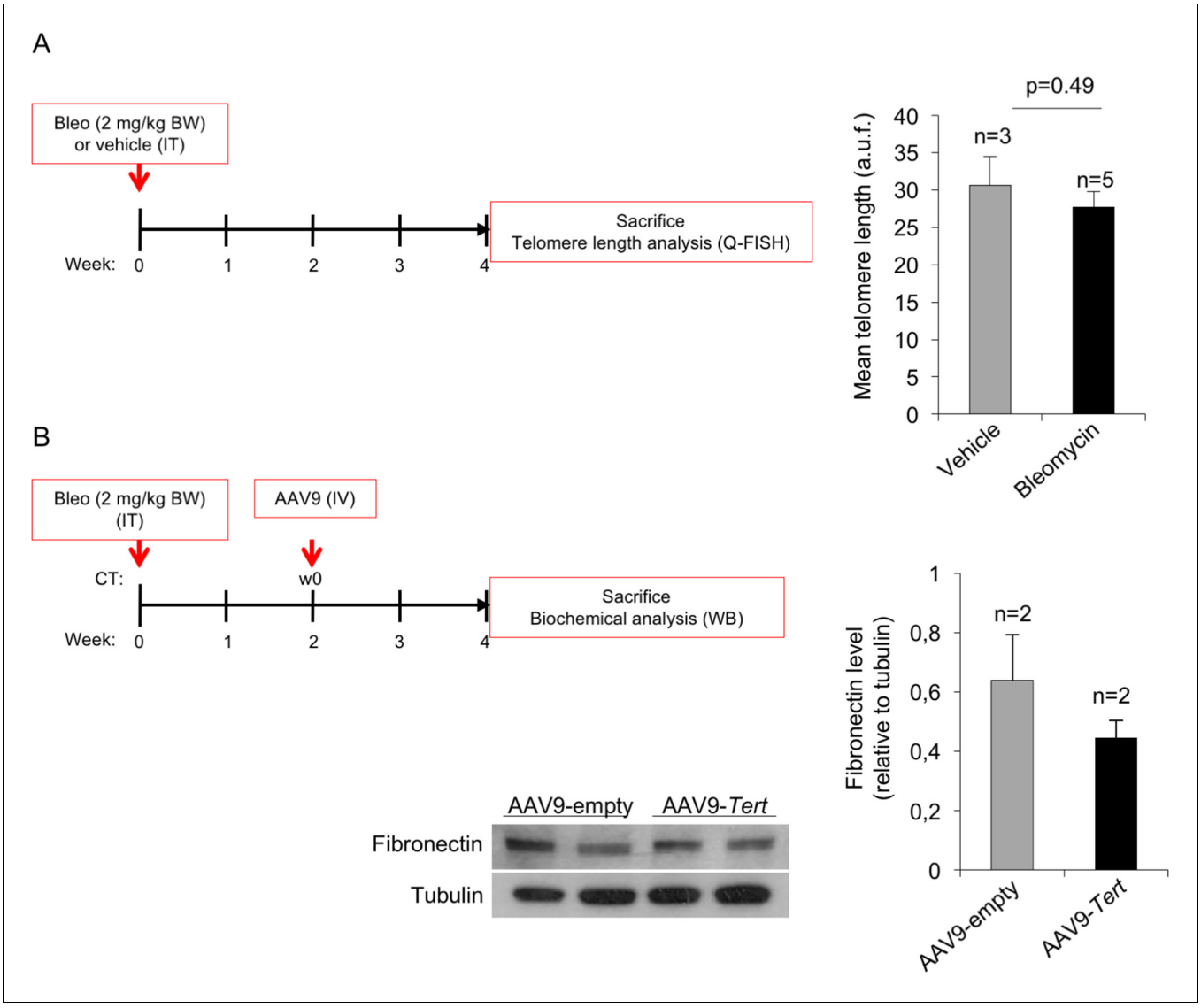

Figure 1—figure supplement 1. High dose of bleomycin induces pulmonary fibrosis without affecting telomere length in lung cells. (**A**) Eight-ten week old wild type mice were intratracheally inoculated either with 2 mg/kg body weight bleomycin or with vehicle and sacrificed after four weeks to measure telomere length by Q-FISH in lung sections (**B**) Eight-ten week old wild type mice were intratracheally inoculated with 2 mg/kg body weight bleomycin and two weeks after computed tomography (CT) diagnosed with pulmonary fibrosis (PF). Affected mice were treated intravenously either with AAV9-Empty or AAV9-*Tert* and sacrificed after two weeks to quantify fibronectin levels by western blot. Representative Western Blot images are shown. T-test was used for statistical analysis. Error bars represent standard error. The number of mice analyzed per group is indicated. a.u.f., arbitrary units of fluorescence.

DOI: https://doi.org/10.7554/eLife.31299.004

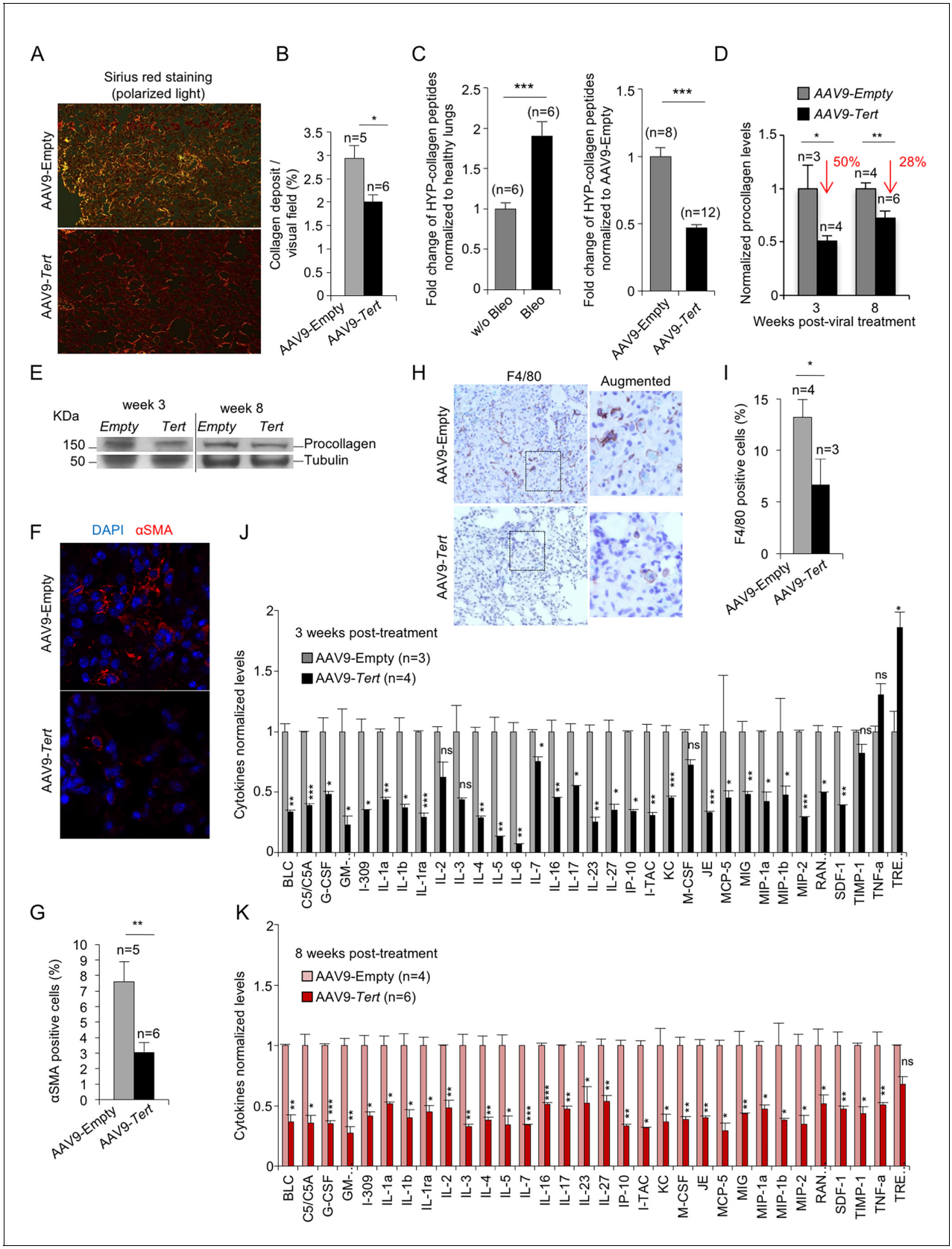

Figure 2. AAV9-*Tert* treatment leads to lower collagen deposition, less inflammation and decreased active fibrotic foci. (**A**) Representative images of picosirius red staining visualized by polarized light where collagen fibers are bright orange from mice treated either with AAV9-*Tert* or empty vector 8

Figure 2 continued on next page

Figure 2 continued

weeks post-viral treatment. (**B**) Percent of lung area filled with collagen fibers 8 weeks post-viral treatment. (**C**) Quantification of specific collagen peptides containing hydroxyproline in healthy lungs without bleomycin and in fibrotic lungs 5 weeks after bleomycin insult (left panel) and in lungs treated either with *Tert* or empty vector at 8 weeks post-treatment (right panel). (**D–E**) Quantification of total procollagen levels (**D**) and representative Western Blot images (**E**) in lung samples of AVV9-*Tert* and AVV9-empty infected lungs at 3 and 8 weeks post-viral treatment. (**F**) Representative images of immunofluorescence for αSMA (in red) and DAPI (in blue) at 8 weeks post-viral treatment. (**G**) Quantification of αSMA positive cells at 8 weeks post-treatment. (**H**) Representative images of F4/80 (macrophage specific marker) immunohistochemistry staining in AAV9-Empty and AAV9-*Tert* treated mice at 8 weeks post-viral treatment. (**I**) Quantification of F4/80 positive cells at 8 weeks post-viral treatment. (**J–K**) Quantification of the indicated cytokines in lung samples of AVV9-*Tert* and AVV9-empty infected lungs at 3 (**J**) and 8 (**K**) weeks post-viral treatment. Data represent the mean ±SE of analyzed mice within each group. The number of mice analyzed per group is indicated. T-test was used for statistical analysis. *p=0.05; **p<0.01; ***p<0.001.

DOI: https://doi.org/10.7554/eLife.31299.005

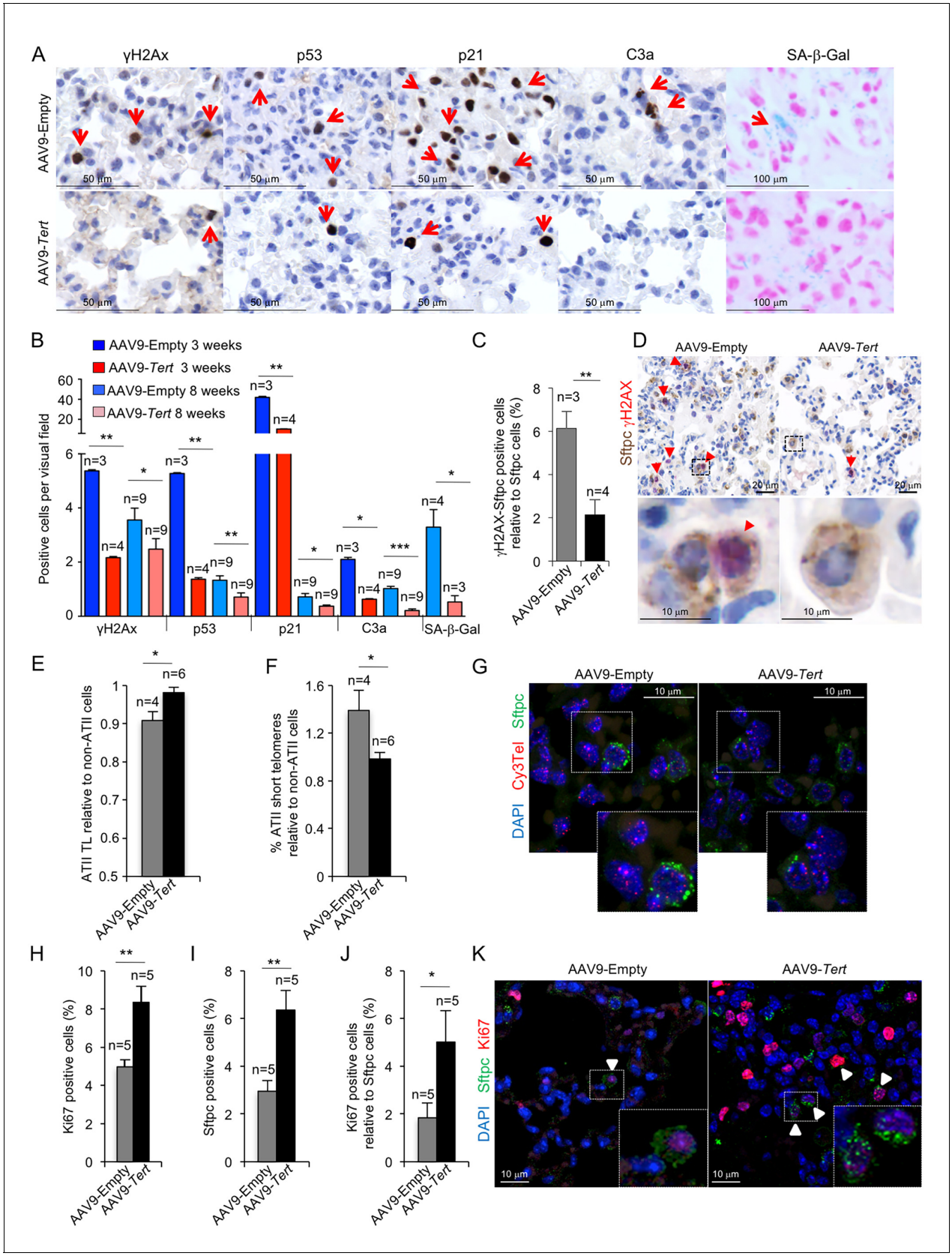

Figure 3. AAV9-*Tert* treatment reduces DNA damage, improves telomere maintenance and proliferation in ATII cells. (**A**) Representative images for γH2AX, p53, p21, active caspase 3 (C3a) and SA-β-Gal stained lungs at 3 weeks post-viral treatment. (**B**) Quantification of γH2AX, p53, p21, C3a and SA-

Figure 3 continued on next page

Figure 3 continued

β-Gal positive cells per visual field of lungs treated either with *Tert* or empty vector at 3 and 8 weeks post-viral treatment. (**C**) percentage of damaged (γH2AX positive) ATII cells (Stfpc positive) in lungs treated either with *Tert* or empty vector at three post-viral treatment. (**D**) Representative images of double immunohistochemistry against Stfpc (brown) and γH2AX (red) of lungs treated either with *Tert* or empty vector at three post-viral treatment. (**E–F**) Fold change in telomere length (**E**) and percentage of short telomeres (**F**) in ATII cells relative to non-ATII cells at 8 weeks post-viral treatment. (**G**) Representative images of immuno-QFISH with Cy3Telomere probe (in red), Sftpc (in green) and DAPI (in blue) in lungs at 8 weeks post-viral treatment. (**H–J**) Quantification of percentage of Ki67 positive cells (**H**), Sftpc positive cells (**I**) and Ki67 positive cells relative to Sftpc positive cells at 8 weeks post-viral treatment (**J**). (**K**) Representative images of double immunofluorescence against Sftpc (in green) and Ki67 (in red) in lungs at 8 weeks post-viral treatment. Data represent the mean ±SE of analyzed mice within each group. The number of mice analyzed per group is indicated. T-test was used for statistical analysis. *p=0.05; **p<0.01; ***p<0.001.

DOI: https://doi.org/10.7554/eLife.31299.006

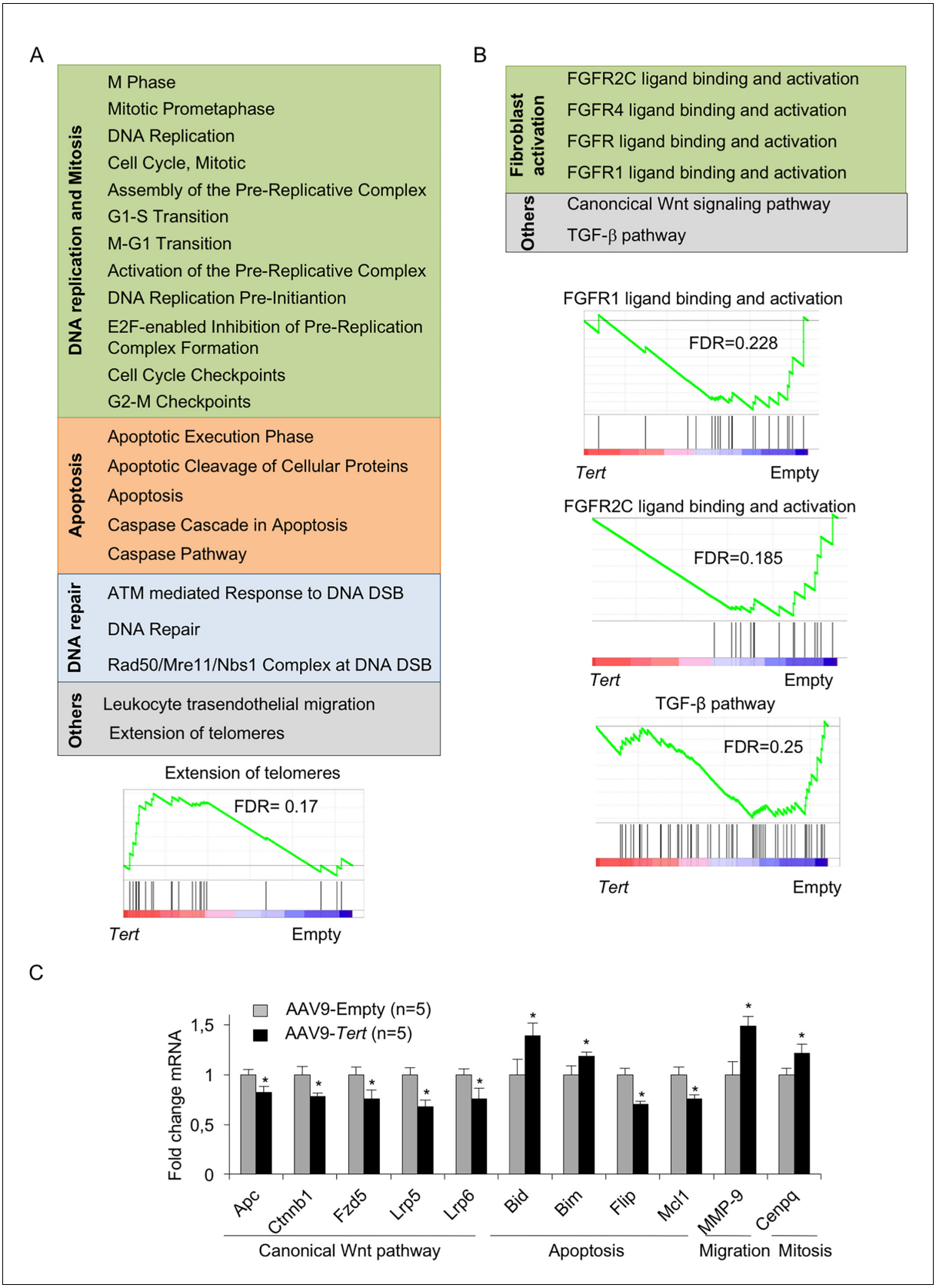

Figure 4. AAV9-*Tert* treatment induces transcriptional changes in the lungs. (**A–B**) Summary table indicating various significantly (FDR < 0.25) upregulated (**A**) and downregulated (**B**) pathways in AAV9-*Tert* compared with AAV9-Empty treated lungs at 8 weeks post-viral treatment. Examples of

Figure 4 continued on next page

Figure 4 continued

GSEA plots for the indicated pathways are shown below. Microarray genes were ranked based on the two-tailed t-statistic tests obtained from the AAV9-*Tert* versus AAV9-Empty by pair-wise comparisons. The red to blue horizontal bar represents the ranked list. Those genes showing higher expression levels for each cohort are located at the edges of the bar (AAV9-Empty; AAV9-*Tert*). The genes located at the central area of the bar show small differences in gene expression fold changes between both groups. (**C**) Fold change mRNA expression levels of candidate genes related with canonical Wnt pathway, apoptosis, mitosis and transendothelial migration in AAV9-*Tert* relative to empty vector. For GSEA Kolmogorov–Smirnoff testing was used for statistical analysis. The FDR is calculated by Benjamini and Hochberg FDR correction. Data represent the mean ± SE of analyzed mice within each group. The number of mice analyzed per group is indicated. T-test was used for q-PCR statistical analysis. *p=0.05.

DOI: https://doi.org/10.7554/eLife.31299.007

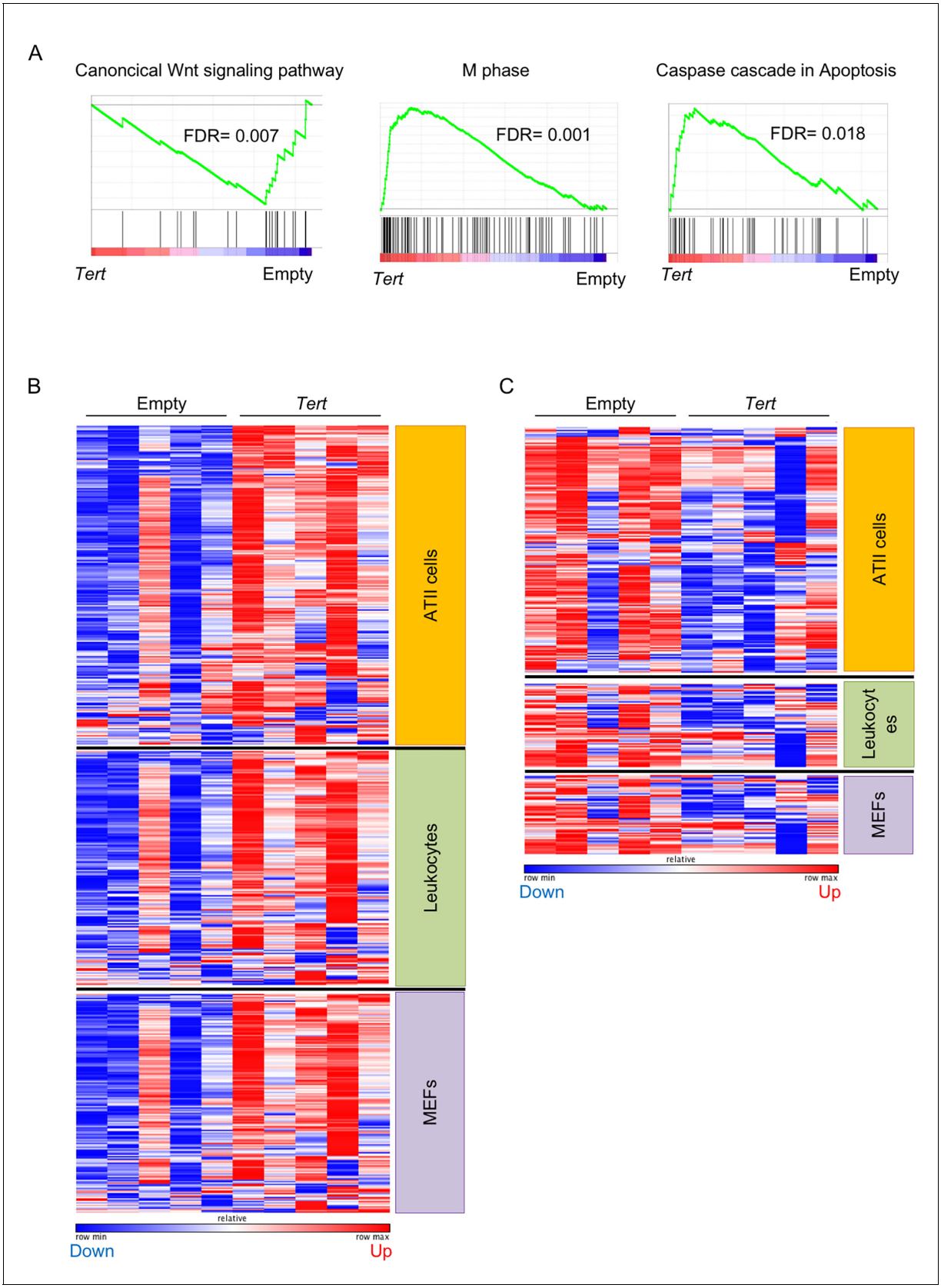

Figure 4—figure supplement 1. Differentially expressed genes from AAV9-*Tert* treated mice correlate with ATII cells gene expression signature. (**A**) GSEA plots for the indicated pathways in lung tissue. Microarray genes were ranked based on the two-tailed t-statistic tests obtained from the AAV9-

Figure 4—figure supplement 1 continued on next page

Figure 4—figure supplement 1 continued

Tert versus AAV9-Empty by pair-wise comparisons. The red to blue horizontal bar represents the ranked list. Those genes showing higher expression levels for each cohort are located at the edges of the bar (AAV9-Empty; AAV9-*Tert*). The genes located at the central area of the bar show small differences in gene expression fold changes between both groups. For GSEA Kolmogorov–Smirnoff testing was used for statistical analysis. The FDR is calculated by Benjamini and Hochberg FDR correction. (**B–C**) Heat maps representing the upregulated genes (**B**) and downregulated genes (**C**) in AAV9-*Tert* compared to empty vector treated mice that corresponded to ATII cells, lung leukocytes and mouse embryonic fibroblast (MEFs). The size of the heat map for each cell type correlates with the amount of genes deregulated. The red/blue bars represent an over/down-expression of the gene in this sample compared with the other cohort.

DOI: https://doi.org/10.7554/eLife.31299.008

A LAD/Sham Haubner´s List

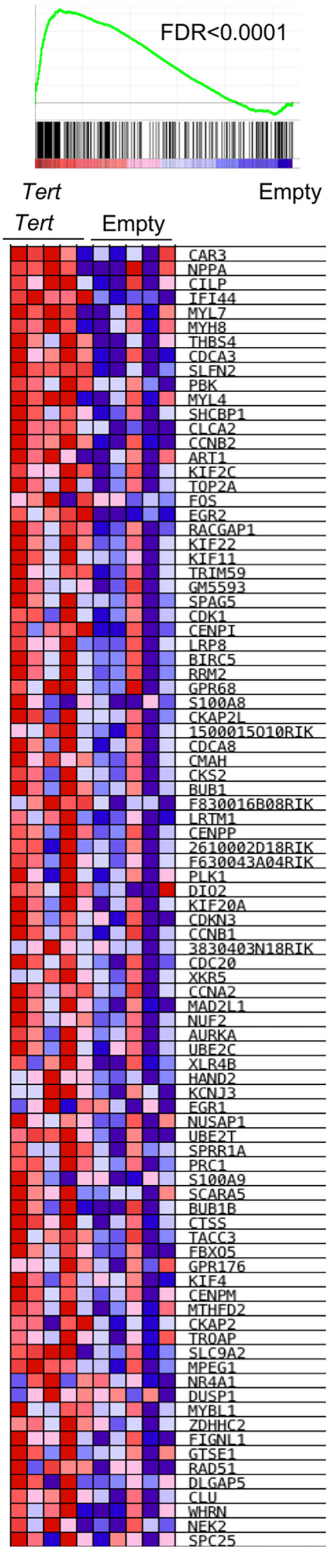

B

Pathways
Activation of NIMA Kinases NEK9, NEK6, NEK7
Nuclear Envelope Breakdown
G1/S Transition
APC/C:Cdh1 mediated degradation of Cdc20 and other APC/C:Cdh1 targeted proteins in late mitosis/early G1
Factors involved in megakaryocyte development and platelet production
Recruitment of mitotic centrosome proteins and complexes
Centrosome maturation
G1/S-Specific Transcription
G0 and Early G1
Nuclear Pore Complex (NPC) Disassembly
Polo-like kinase mediated events
Condensation of Prophase Chromosomes
Mitotic Prophase
G2/M Checkpoints
Deposition of new CENPA-containing nucleosomes at the centromere
Nucleosome assembly
Loss of proteins required for interphase microtubule organization from the centrosome
Loss of Nlp from mitotic centrosomes
Condensation of Prometaphase Chromosomes
Conversion from APC/C:Cdc20 to APC/C:Cdh1 in late anaphase
Depolymerisation of the Nuclear Lamina
Mitotic Telophase/Cytokinesis
MASTL Facilitates Mitotic Progression
Recruitment of NuMA to mitotic centrosomes
E2F-enabled inhibition of pre-replication complex formation
G2/M DNA replication checkpoint
G2/M DNA damage checkpoint
Chk1/Chk2(Cds1) mediated inactivation of Cyclin B:Cdk1 complex
Cyclin B2 mediated events

Pathways
Resolution of Sister Chromatid Cohesion
Mitotic Prometaphase
M Phase
Mitotic Metaphase and Anaphase
Separation of Sister Chromatids
Mitotic Anaphase
Regulation of mitotic cell cycle
APC/C-mediated degradation of cell cycle proteins
Activation of APC/C and APC/C:Cdc20 mediated degradation of mitotic proteins
Regulation of APC/C activators between G1/S and early anaphase
APC/C:Cdc20 mediated degradation of mitotic proteins
APC:Cdc20 mediated degradation of cell cycle proteins prior to satisfation of the cell cycle checkpoint
APC-Cdc20 mediated degradation of Nek2A
Cyclin A/B1 associated events during G2/M transition
Kinesins
Cdc20:Phospho-APC/C mediated degradation of Cyclin A
Cell Cycle Checkpoints
G2/M Transition
Mitotic G2-G2/M phases
Regulation of PLK1 Activity at G2/M Transition
Phosphorylation of the APC/C
Inhibition of the proteolytic activity of APC/C required for the onset of anaphase by mitotic spindle checkpoint components
Inactivation of APC/C via direct inhibition of the APC/C complex
Phosphorylation of Emi1
Mitotic Spindle Checkpoint
APC/C:Cdc20 mediated degradation of Cyclin B
Golgi Cisternae Pericentriolar Stack Reorganization
MHC class II antigen presentation
E2F mediated regulation of DNA replication
Mitotic G1-G1/S phases

Figure 4—figure supplement 2. *Tert* overexpression in fibrotic lungs mimic neonatal regenerative heart tissue after infarctation. (**A**) GSEA plot for LAD/Sham List from Haubner *et al.* study. A heatmap of indicated core-enriched genes is displayed under the enrichment plot. Microarray genes were

Figure 4—figure supplement 2 continued on next page

Figure 4—figure supplement 2 continued

ranked based on the two-tailed t-statistic tests obtained from the AAV9-*Tert* versus AAV9-Empty by pair-wise comparisons. The red to blue horizontal bar represents the ranked list. Those genes showing higher expression levels for each cohort are located at the edges of the bar (AAV9-Empty; AAV9-Tert). The genes located at the central area of the bar show small differences in gene expression fold changes between both groups. (**B**) REACTOME Pathways differentially enriched with genes of the core-enriched from the previous GSEA. For GSEA Kolmogorov–Smirnoff testing was used for statistical analysis. The FDR is calculated by Benjamini and Hochberg FDR correction.

DOI: https://doi.org/10.7554/eLife.31299.009

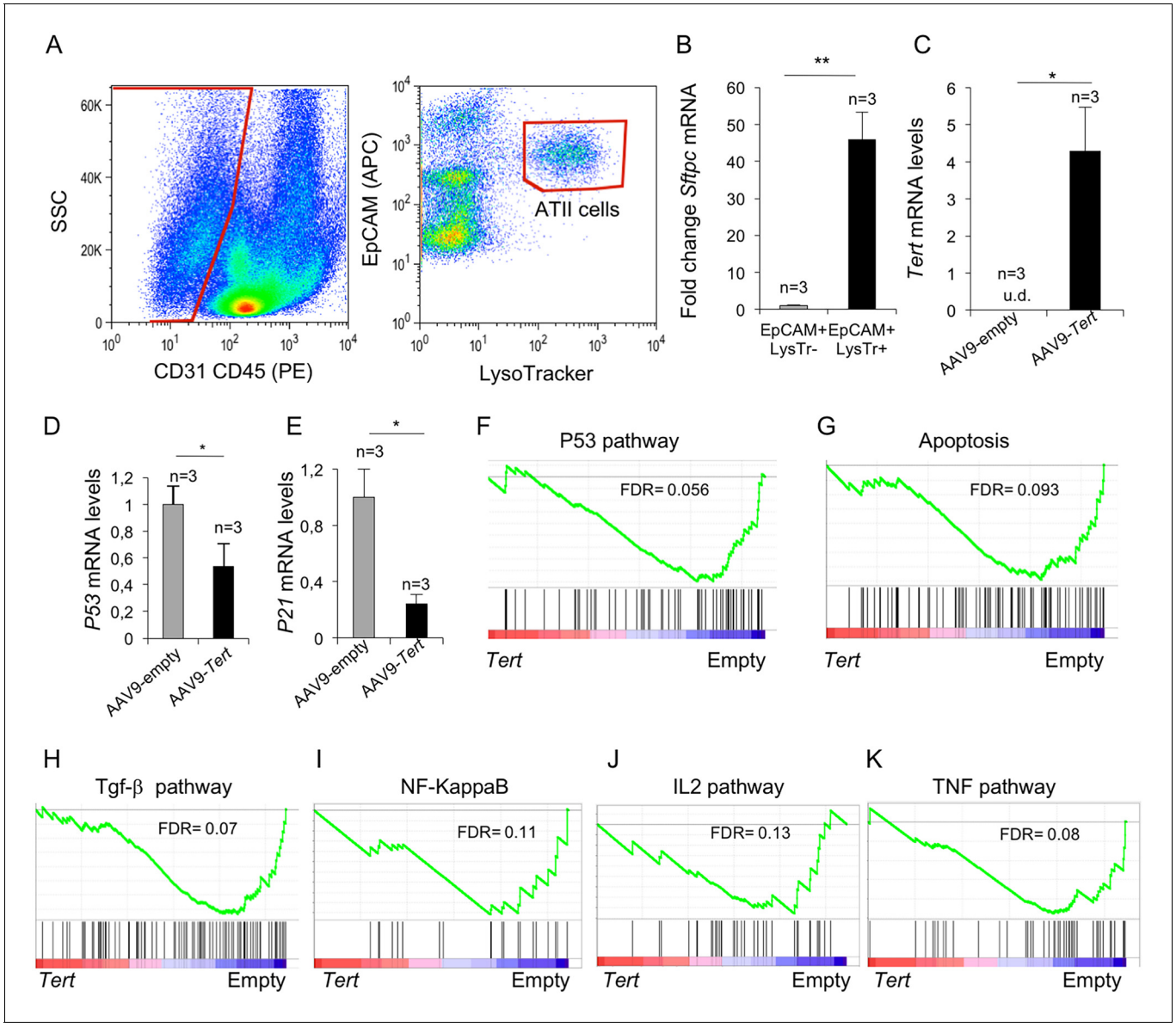

Figure 5. Isolated ATII cells overexpress *Tert* and show downregulation of DDR- and inflammatory- related pathway. (**A**) FACs representative dot plots of lungs one week post either AAV9-Empty or AAV9-*Tert* treatment. The epithelial cell population was identified as CD31/CD45 double negative. ATII cells were identified by LysoTracker and EpCAM doubly positive cells and isolated by cell sorting. (**B**) Validation of specific ATII cells marker *Sftpc* by RT-qPCR. (**C**) Transcriptional levels of *Tert* in isolated ATII cells from lungs treated with the indicated vectors. (**D–E**) mRNA expression levels of *p53* (**C**) and *p21* (**D**) genes in ATII by RT-qPCR from lungs treated with the indicated vectors. (**F–G**) GSEA plots for the indicated downregulated DDR related pathways in AAV9-*Tert* infected ATII cells. (**H–K**) GSEA plots for the indicated downregulated inflammatory related pathways in AAV9-*Tert* infected ATII cells. Microarray genes were ranked based on the two-tailed t-statistic tests obtained from the AAV9-*Tert* versus AAV9-Empty by pair-wise comparisons. The red to blue horizontal bar represents the ranked list. Those genes showing higher expression levels for each cohort are located at the edges of the bar (AAV9-Empty; AAV9-*Tert*). The genes located at the central area of the bar show small differences in gene expression fold changes between both groups. Data represent the mean ±SE of analyzed mice within each group. The number of mice analyzed per group is indicated. T-test was used for RT-qPCR statistical analysis. *p=0.05; **p<0.01. For GSEA Kolmogorov–Smirnoff testing was used for statistical analysis. The FDR is calculated by Benjamini and Hochberg FDR correction.

DOI: https://doi.org/10.7554/eLife.31299.010

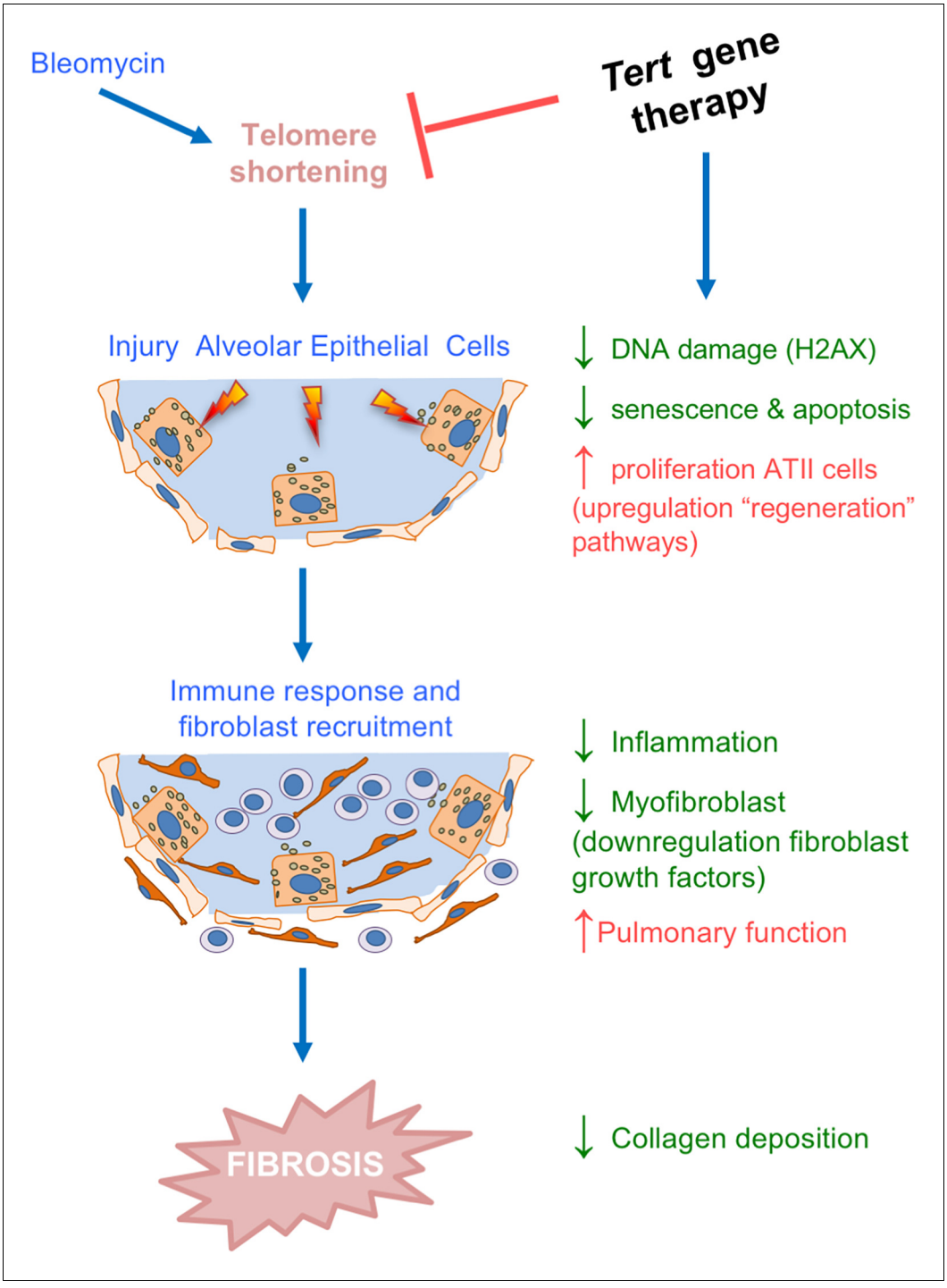

Figure 6. *Tert* gene therapy targets the basis of pulmonary fibrosis. Proposed model for the mechanism underlying *Tert* gene therapy. AAV9-*Tert* therapy targets one of the molecular causes of the disease, short telomeres (***Alder et al., 2008***; ***Armanios et al., 2007***; ***Povedano et al., 2015***), resulting in decreased DNA damage, senescence/apoptosis and improved proliferative potential of the ATII cells and subsequently decreasing inflammation and fibrosis.

DOI: https://doi.org/10.7554/eLife.31299.011